

AperTO - Archivio Istituzionale Open Access dell'Università di Torino

## Structural and spectroscopic properties of high temperature prepared ZrO<sub>2</sub>-TiO<sub>2</sub> mixed oxides

### This is the author's manuscript

*Original Citation:*

*Availability:*

This version is available <http://hdl.handle.net/2318/130771> since

*Published version:*

DOI:10.1016/j.jssc.2013.02.040

*Terms of use:*

Open Access

Anyone can freely access the full text of works made available as "Open Access". Works made available under a Creative Commons license can be used according to the terms and conditions of said license. Use of all other works requires consent of the right holder (author or publisher) if not exempted from copyright protection by the applicable law.

(Article begins on next page)



# UNIVERSITÀ DEGLI STUDI DI TORINO

*This is an author version of the contribution published on:*

*Questa è la versione dell'autore dell'opera:*

*Journal of Solid State Chemistry 201 (2013) 222–228*

*Chiara Gionco, Alfio Battiato, Ettore Vittone, Maria Cristina Paganini,  
Elio Giamello*

*doi.org/10.1016/j.jssc.2013.02.040*

*The definitive version is available at:*

*La versione definitiva è disponibile alla URL:*

<http://www.sciencedirect.com/science/journal>

# Structural and spectroscopic properties of high temperature prepared $ZrO_2$ - $TiO_2$ mixed oxides.

Chiara Gionco<sup>a</sup>, Alfio Battiato<sup>b</sup>, Ettore Vittone<sup>b</sup>, Maria Cristina Paganini<sup>a\*</sup>, Elio Giamello<sup>a</sup>

<sup>a</sup>Dipartimento di Chimica and NIS (Nanostructured Surfaces and Interfaces), Università degli Studi di Torino, Via Giuria 7, 10125 Torino, Italy

<sup>b</sup>Dipartimento di Fisica, Università degli Studi di Torino, Via Giuria 1, 10125 Torino, Italy

## ***Abstract***

$ZrO_2$ - $TiO_2$  mixed oxides of various composition, with the molar fraction of  $TiO_2$  ranging from 0.1% to 15%, have been prepared via sol-gel synthesis and then calcined at 1273K to check both their thermal stability and physicochemical properties. These solids are usually employed in photocatalytic processes and as active phase supports in heterogeneous catalysis. As indicated by X-ray diffraction and Raman spectroscopy, solid solutions based on Ti ions diluted in the  $ZrO_2$  matrix are formed in the whole range of Ti molar fraction examined. Materials with low Ti loading (0.1%-1%) are basically constituted by the monoclinic phase of  $ZrO_2$  while the tetragonal phase becomes prevalent at 15% of  $TiO_2$  molar fraction. The presence of Ti ions modify the electronic structure of the solid as revealed by investigation of the optical properties. The typical band gap transition of  $ZrO_2$  undergoes, in fact, a red shift roughly proportional to the Ti loading which reach the remarkable value of 1.6 eV for the sample with 10% of molar Ti concentration. Comparing chemical analysis of the solids with XPS data it has been put into evidence that the titanium ions distribution into the solid is not uniform and the concentration of  $Ti^{4+}$  tend to be higher in subsurface layers than in the crystal bulk. The introduction of titanium ions in the structure increases the reducibility of the solid. Annealing under vacuum at various temperatures causes oxygen depletion with consequent reduction of the solid which shows up mainly in terms of formation of  $Ti^{3+}$  reduced centres which are characterized by a typical EPR signal.  $Ti^{3+}$  defects forms, as also forecast by theoretical modelling of the solid, as their energy is lower than that of other possible reduced defective centers. The reduced solids are able to transfer electrons to adsorbed oxygen molecules in mild condition resulting in the formation of surface superoxide anions ( $O_2^{\bullet-}$ ) which are stabilized on surface  $Zr^{4+}$  or, alternatively, on  $Ti^{4+}$  ions according to the sample composition.

KEYWORDS: Mixed oxides, oxygen depletion and reducibility, EPR,  $TiO_2$ ,  $ZrO_2$ .

To whom correspondence should be addressed: Maria Cristina Paganini, via Giuria 7, 10125  
Torino, Italy, phone +39-011-6707576, fax +39-011-6707855, e-mail:

[mariacristina.paganini@unito.it](mailto:mariacristina.paganini@unito.it)

## 1. Introduction

Zirconium dioxide is a strategic material which attracted a great deal of interest in the past few decades because of the large range of applications in the fields of ceramic compounds, optical devices, gas sensors and catalysis<sup>1</sup>. There are three main polymorphs of pure ZrO<sub>2</sub> whose structures are respectively monoclinic (stable up to 1443K), tetragonal (stable from 1443K to 2643K) and cubic (stable at high temperature from 2643K up to the melting temperature at 2979K)<sup>2</sup>. An additional metastable tetragonal phase (up to 650°C) is also reported whose formation, in preparations involving moderate calcinations temperature of precursors aiming to obtain high surface area systems, has been attributed either to impurity effects or to crystallite size effects<sup>1</sup>. For several applications the use of tetragonal or cubic phases is required to avoid phase transformations caused by temperature. Stable tetragonal and cubic zirconia are obtained via doping with Y<sub>2</sub>O<sub>3</sub> (t-ZrO<sub>2</sub>) or CaO (c-ZrO<sub>2</sub>) both causing the formation of anion vacancies in the system. High surface area ZrO<sub>2</sub> has low thermal stability and, when calcined at high temperatures, undergoes a phase transition from tetragonal to monoclinic accompanied by a drastic decrease in surface area. Therefore, several attempts have been made to improve the ZrO<sub>2</sub> thermal stability also by incorporation of isovalent ions like Ce and/or Ti<sup>3-5</sup> which, in principle, do not generate anion vacancies. ZrO<sub>2</sub>-TiO<sub>2</sub> mixed oxides have been studied in recent years because they show both better thermal stability and modified surface acidity properties with respect to the bare ZrO<sub>2</sub><sup>4,6</sup> and they are therefore used, like the parent material, as catalysts and catalyst supports for various catalytic reactions such as dehydrogenation<sup>7,8</sup> and isomerisation<sup>9,10</sup>. Several examples of photocatalytic applications of this mixed oxide are also available<sup>11-16</sup>. A relatively large number of studies have been thus devoted to the preparation of ZrO<sub>2</sub>-TiO<sub>2</sub> mixed materials<sup>17,18</sup> under the form of powders or of thin films. In spite of this fact the papers devoted to the characterization of this system are relatively few<sup>4,6,19-23</sup> and a thorough investigation of the general physico-chemical properties of ZrO<sub>2</sub>-TiO<sub>2</sub> (optical properties, redox behaviour, surface reactivity) is substantially still lacking. Such an activity has been probably conditioned by the frequent formation of mixtures of zirconia polymorphs which add an undesired complexity to the system limiting basic research studies.

In a recent preliminary investigation by some of us<sup>19</sup> the metastable tetragonal phase of ZrO<sub>2</sub>-TiO<sub>2</sub> was investigated in order to gain information on the influence of titanium on the properties of the matrix in a system displaying a high specific surface area, prepared in mild temperature conditions. This study, though influenced by the metastable nature of the phase well described by Ondik<sup>24</sup> in the ZrO<sub>2</sub>-TiO<sub>2</sub> phase diagram, has shown the capability of titanium impurities to modify the electronic structure of zirconia causing a net reduction of its band gap,

moreover a wider region of stability for the metastable tetragonal phase is expected for Ti higher amount.

In the present paper we report an investigation of ZrO<sub>2</sub>–TiO<sub>2</sub> mixed oxides containing a fraction of TiO<sub>2</sub> ranging from 0.1% to 15 mol% which have been prepared by sol-gel synthesis. The synthesized materials have been calcined at 1273K for 48 hours with the aim of overcoming the formation of a metastable phase and if possibly obtaining a single and stable crystallographic phase either monoclinic (lower Ti loadings) or a mixture of monoclinic and tetragonal (higher Ti molar fraction). A complete characterization of the variously loaded materials has been performed using several structural and optical techniques. In this work, in particular, the reducibility of the solid by oxygen depletion has been studied. This property is of capital importance in many catalytic phenomena as it is related to the reactivity of the oxide. ZrO<sub>2</sub> has a relevant band gap (around 5eV) and its capability of loosing oxygen is relatively modest and, in any case, lower than that of typical semiconducting oxides. In the mentioned previous work<sup>19</sup> we found an influence of titanium in increasing the capability of oxygen depletion of the solid. This phenomenon however must be confirmed on a crystallographic better defined matrix.

A particular role is assumed, in this part of investigation, by Electron Paramagnetic Resonance (EPR). EPR is the reference technique to study paramagnetic defects in solids and electron transfer processes leading to molecules in paramagnetic state<sup>25, 26</sup>. We have employed EPR to monitor, on one hand, the presence of reduced paramagnetic centres in the lattice after annealing and, on the other hand, to investigate the electron transfer from the reduced solid to surface adsorbed oxygen to give O<sub>2</sub><sup>•-</sup> radical anions. These radical anions also play the role of probe of the surface adsorption sites providing information on the nature of surface active sites.

## ***2. Material and methods***

### ***2.1. Preparation of the samples***

All reactants employed in this work were purchased by Aldrich and used without any further purification treatment. Double distilled water was used in the synthesis procedures. ZrO<sub>2</sub> and the ZrO<sub>2</sub>/TiO<sub>2</sub> samples were prepared following the sol-gel route described by Livraghi et al.<sup>19</sup>. To prepare the bare ZrO<sub>2</sub> a solution containing zirconium propoxide, 2-propanol (with alkoxide/alcohol molar ratio 1:4) and water (alcohol/water ratio 1:2) was prepared stirring continuously at room temperature. The gel formed was aged over night, then dried in oven at 50°C. For the mixed samples the stoichiometric amount of titanium isopropoxide was added into the solution. The concentration of the mixed oxides was 0.1, 1, 10 and 15% molar of TiO<sub>2</sub> in ZrO<sub>2</sub>. After drying all samples were then heated up to 1273K for 48 hours. The samples will

be referred to as ZT followed by the molar concentration of titanium (Z stands for the pure ZrO<sub>2</sub> sample).

## 2.2. Characterization of the materials

Powder x-rays diffraction (XRD) patterns were recorded with a PANalytical PW3040/60 X'Pert PRO MPD using a copper K $\alpha$  radiation source (0.15418 nm) and a X'Pert High-Score software for data handling. Rietveld refinement was performed on the diffraction patterns was used to determine the crystallite size and relative abundance of phases, using the MAUD 2.26 software and a NIST Si powder to determine the instrumental broadening.

The UV-Vis absorption spectra were recorded using a Varian Cary 5 spectrometer, coupled with an integration sphere for diffuse reflectance (DR) studies, using a Carywin-UV/scan software. A sample of PTFE with 100% reflectance was used as reference.

$\mu$ -Raman spectra were recorded on a Jobin Yvon LabRam HR800 Raman Spectrometer, equipped with a He-Ne laser (632.8 nm), connected to an Olympus BX41 microscope. Spectra were recorded using a 600 $\mu$ m hole at a 50X magnification.

EPR spectra recorded at room temperature and at liquid nitrogen temperature were run on a X-band CW-EPR Bruker EMX spectrometer equipped with a cylindrical cavity operating at 100 kHz field modulation.

X-ray Photoelectron Spectroscopy (XPS) analysis were performed using a VSW TA10 non-monochromatic Al K $\alpha$  x-ray source equipped with a VSW Class 100 Concentric Hemispherical Analyzer.

## **3. Results and discussion**

### 3.1. Structural characterization

X-ray diffraction analysis was performed to check the crystalline phases present in the samples after synthesis. The diffraction patterns of the mixed samples are shown in Fig. 1.

The figure indicates that the monocline polymorph of ZrO<sub>2</sub> is the dominant phase for low Ti loading samples (ZT01, ZT1). The diffraction peaks are narrow, indicating the formation of large crystallites. For materials with high Ti concentration the presence of the tetragonal phase becomes more important, as, by the way, expected on the basis of the state diagram of the ZrO<sub>2</sub>-TiO<sub>2</sub> system<sup>24</sup> and it is dominant in the case of ZT15. For this sample XRD peaks are broadened indicating that the crystallites are smaller than those of all other samples. None of the samples here examined exhibit peaks indicating the presence of phases amenable to some TiO<sub>2</sub> polymorph. This seems to suggest (*vide infra*) the formation of a solid solution between the two components<sup>4, 22</sup>.

Fig. 1

On all XRD patterns a Rietveld refinement with the MAUD software was performed<sup>27, 28</sup>. The results concerning the crystallite size, the cell parameters and the relative abundance of the different phases are reported in Table 1. The lattice parameters are scarcely modified by the incorporation of the Ti ion, whereas the abundance of the tetragonal polymorph present in the mixture and the size of the crystallites are heavily dependent on Ti concentration. The crystallite size decreases for both zirconia phases (m and t) with increasing the Ti content except in the case of the monoclinic phase in ZT15 for which the crystallite size and the tetragonal polymorph abundance increases again.

Sample	a [Å]	b [Å]	c [Å]	$\beta$ [°]	%wt	d [Å]
<b>Z</b>						
t-ZrO <sub>2</sub>	3.5971 ±0.0006	3.5971 ±0.0006	5.1867 ±0.0017	/	2.34	970 ±60
m-ZrO <sub>2</sub>	5.14675 ±0.00009	5.20533 ±0.0001	5.31857 ±0.00009	99.1729 ±0.0012	97.66	1825 ±16
<b>ZT01</b>						
t-ZrO <sub>2</sub>	3.5991 ±0.0003	3.5991 ±0.0003	5.1943 ±0.0007	/	7.24	1080 ±50
m-ZrO <sub>2</sub>	5.15081 ±0.00010	5.21196 ±0.00011	5.32144 ±0.00011	99.1873 ±0.0014	92.76	1235 ±9
<b>ZT1</b>						
t-ZrO <sub>2</sub>	3.584 ±0.010	3.584 ±0.010	5.15 ±0.03	/	2.36	280 ±110
m-ZrO <sub>2</sub>	5.14907 ±0.00010	5.20430 ±0.00010	5.32347 ±0.00011	99.1799 ±0.0014	97.64	1170 ±11
<b>ZT10</b>						
t-ZrO <sub>2</sub>	3.58822 ±0.00015	3.58822 ±0.00015	5.1963 ±0.0004	/	34.35	353 ±2
m-ZrO <sub>2</sub>	5.1338 ±0.0003	5.1778 ±0.0004	5.3196 ±0.0003	99.884 ±0.004	65.65	514 ±4
<b>ZT15</b>						
t-ZrO <sub>2</sub>	3.58221	3.58221	5.20187	/	95.47	433

	$\pm 0.00007$	$\pm 0.00007$	$\pm 0.00019$			$\pm 3$
m-ZrO <sub>2</sub>	5.1293	5.1994	5.3215	99.055	4.53	1900
	$\pm 0.0016$	$\pm 0.0016$	$\pm 0.0015$	$\pm 0.014$		$\pm 400$

**Table 1.** Cell parameters, weight percentage and crystallite size obtained from Rietveld refinement of XRD patterns in Fig. 1.; a, b and c are lattice parameters,  $\beta$  is the angle between a and c axes for the monoclinic cell, %wt is the weight percentage of a given phase, d is the crystallite size.

Figure 2 shows the  $\mu$ -Raman spectra obtained for all ZT samples. Each spectrum is the average between five acquisitions that were made at different points of the sample to check its homogeneity.  $\mu$ -Raman is a bulk technique but, since it samples specific parts of the sample, it also is a local probe.

Raman spectroscopy, furthermore, is an extremely sensitive method to determine the phase composition in the case of many transition metal oxides. For tetragonal ZrO<sub>2</sub> six Raman-active modes are expected, namely 147 cm<sup>-1</sup> (B<sub>1g</sub>), 261 cm<sup>-1</sup> (E<sub>g</sub>), 318 cm<sup>-1</sup> (B<sub>1g</sub>), 463 cm<sup>-1</sup> (E<sub>g</sub>), 611 cm<sup>-1</sup> (A<sub>1g</sub>), 641 cm<sup>-1</sup> (E<sub>g</sub>)<sup>19, 29-31</sup>. For the monoclinic phase of ZrO<sub>2</sub> the theory forecasts eighteen Raman-active modes. Fourteen of those modes are in the range 100÷800cm<sup>-1</sup> here explored, namely at 176 cm<sup>-1</sup>(A<sub>g</sub>), 187 cm<sup>-1</sup>(A<sub>g</sub>), 220 cm<sup>-1</sup>(B<sub>g</sub>), 300 cm<sup>-1</sup>(A<sub>g</sub>), 333 cm<sup>-1</sup>(B<sub>g</sub>), 344 cm<sup>-1</sup>(B<sub>g</sub>), 380 cm<sup>-1</sup>(B<sub>g</sub>), 475 cm<sup>-1</sup>(A<sub>g</sub>), 510 cm<sup>-1</sup>(B<sub>g</sub>), 536 cm<sup>-1</sup>(B<sub>g</sub>), 558 cm<sup>-1</sup>(A<sub>g</sub>), 613 cm<sup>-1</sup>(B<sub>g</sub>), 635 cm<sup>-1</sup>(A<sub>g</sub>), 760 cm<sup>-1</sup>(A<sub>g</sub>)<sup>19, 29-31</sup>.

**Fig. 2.**

The  $\mu$ -Raman results are in good agreement with those of the XRD patterns as only ZrO<sub>2</sub> phases are detected. The sensitivity of Raman spectroscopy is particularly high in the case of TiO<sub>2</sub> polymorphs as both rutile and anatase show particularly intense and characteristic peaks (144 and 639 cm<sup>-1</sup> for anatase, 447 and 612 cm<sup>-1</sup> for rutile respectively)<sup>32, 33</sup>. The absence of such Raman peaks in the spectra conclusively allows to exclude the presence of segregated TiO<sub>2</sub> in all prepared materials. Since titanium is effectively present in all these materials we can reasonably conclude that the preparation method adopted led to the formation of solid solutions with titanium ions diluted in ZrO<sub>2</sub> matrices. According to the phase diagram, 10% of Ti molar fraction is the limiting value for the formation of the tetragonal phase. For this reason in Fig.2, two different spectra for ZT10 ( a borderline case) are reported sampling two different regions of the material. In one case (Fig. 2d)

the monoclinic phase is observed while in the other spectrum (Fig. 2d') the tetragonal phase appears.

### 3.2 Optical characterization

All prepared materials were investigated by DR-UV-Vis spectroscopy in order to unravel differences in their electronic structure. Typical UV-VIS absorption spectra, calculated by using the Kubelka–Munk function  $[F(R_{\infty})]$ , are shown in Fig. 3, where the typical spectrum of a TiO<sub>2</sub> sample (rutile) is also reported for sake of comparison. For both ZT01 and ZT1 three absorption bands in the near UV are observed. Their presence, and the absence of the typical edge in the case of ZT1 (Fig.3 c), are related to photoluminescence effects whose investigation is not among the scopes of the present paper. Despite the interference of the photoluminescence, the valence band to conduction band transition typical of ZrO<sub>2</sub> seems not to be affected in these two cases. As opposite, in the case of high loading materials (ZT10 and ZT15) a dramatic red shift of the absorption edge is clearly visible which is nearly the same in the two cases. A similar behaviour, indicating a substantial reduction of the band gap, was already reported by some of us for systems prepared at different temperature<sup>19</sup> even though, in the present case, the shift is even more evident.

#### **Fig. 3.**

Energy gap values have been calculated by linearization of the plot reporting  $(\alpha h\nu)^{1/2}$  vs  $h\nu$  typical of indirect band gap transitions<sup>34</sup>. For the bare zirconia (Z, Fig 3B, a) the observed energy gap is 5.0 eV while for ZT10 (the sample with the highest red shift) is 3.4 eV. The band gap narrowing shown by this sample, and related to the presence of 10% of Ti ions, reaches the remarkable value of 1.6 eV indicating that the inclusion of Ti ions into the lattice, strongly modifies the electronic structure of the materials. The progressive band gap red shift increases with increasing titanium concentration from ZT01 to ZT10 (essentially monoclinic phase). This trend is, of course, not valid for ZT15 (tetragonal phase).

### 3.3 XPS spectroscopy

XPS measurements were carried out in order to monitor the material composition in the surface and subsurface region of about a few nm in depth covered by this kind of analysis. The core lines position has been evaluated with respect to the adventitious C 1s peak at 285 eV. A survey spectrum of ZT10 is shown in Fig. 4 and the results on the composition of all samples are reported in Table 2. In parallel an ICP chemical analysis was performed to monitor the composition of the whole materials (results also reported in Table 2). ICP analysis shows that the real composition of each

material is in substantial agreement with the nominal one. As opposite the surface composition monitored by XPS diverges from the chemical analysis indicating a higher concentration of Ti ions in the external part of the crystals. In spite of the preparation method (intimate mixture at the liquid state of the two basic components and final thermal treatment at high temperature) the crystals seem not fully homogeneous and a gradient in the Ti ions concentration going from the surface to the bulk of the particles is suggested by comparison of the two types of analysis.

**Fig. 4**

Sample	Nominal Ti/Zr ratio	ICP Ti/Zr ratio	XPS Ti/Zr ratio
ZT01	0.001	0.002±0.001	0.020±0.003
ZT1	0.010	0.010±0.001	0.080±0.008
ZT10	0.100	0.091±0.008	0.29±0.02
ZT15	0.150	0.151±0.015	0.34±0.03

**Table 2. Nominal composition of the samples compared to those monitored by ICP (stoichiometric analysis) and XPS (surface analysis)**

### 3.4 EPR Spectroscopy

EPR spectroscopy is one of the most suitable techniques to investigate defects in materials. We have investigated by EPR the samples prepared in this work in order to monitor their reducibility. Several transition metal oxides in fact show oxygen depletion upon annealing under vacuum with consequent formation of excess electrons in the solid which can, in some instances, be stabilized by particular metal ions capable of undergoing reduction. The redox properties of these reducible oxides are important in many catalytic processes. The base lines of the EPR spectra of the as prepared samples (not shown for sake of brevity) are not completely flat as they show a very weak signal with axial symmetry ( $g_{\parallel}=1.978$  and  $g_{\perp}=1.960$ ), assigned in literature to  $Zr^{3+}$  ion<sup>19, 35-39</sup> and indicating a tiny deviation from the stoichiometry corresponding to a full oxidation. Figure 5 shows the spectra obtained on the samples annealed for 1 hour at 873K under dynamic vacuum. Low loading mixed samples (ZT01 and ZT1) behave in a similar way to bare zirconia. An isotropic signal with  $g=2.003$  in fact appears and simultaneously all other signals disappear<sup>19, 35, 38, 39</sup>. For samples with high Ti loading (ZT10 and ZT15) the isotropic signal is accompanied by a broad axial signal amenable to the formation of  $Ti^{3+}$  ions (Fig. 5d, e)<sup>19</sup>. Fig. 6 reports the experimental spectra of the vacuum annealed ZT10 and ZT15 materials together with their computer simulation. Both

spectra are characterised by the presence of two distinct axial species (see Table 3) one of which is common to both samples (species A) and is probably due to  $\text{Ti}^{3+}$  ions at the surface or close to it in a slightly distorted environment. The other two species are preliminarily associated to  $\text{Ti}^{3+}$  in the cationic site of tetragonal zirconia (species B, sample ZT15) and to the same ion in monoclinic zirconia (species C, sample ZT10). The spectrum related to the reduced ZT15 sample (Fig 6 B) is the same observed in low temperature prepared  $\text{TiO}_2\text{-ZrO}_2$  materials<sup>19</sup> which also contains predominantly the tetragonal phase.

Fig. 5

Fig. 6

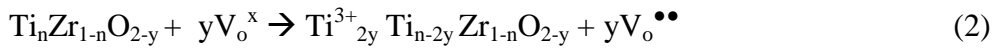
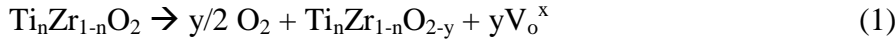
Species	$g_{\parallel}$	$g_{\perp}$	sample	assignment
A	1.978	1.905	ZT10, ZT15	Surface and subsurface
B	1.967	1.929	ZT15	$\text{Ti}^{3+}$ in t- $\text{ZrO}_2$
C	1.958	1.918	ZT10	$\text{Ti}^{3+}$ in m- $\text{ZrO}_2$

**Table 3. Spin Hamiltonian parameters of the species A, B, and C present in the EPR spectra of reduced ZT10 and ZT15, g-factors obtained via computer simulation.**

Since the amount of reduced centres drastically increases passing from Z to ZT15 (Figs 5 and 6) at first sight the effect of Ti insertion seems to be that of an augmentation of the reducibility of the material. This is not surprising since the reducibility of an oxide tends to decrease with increasing the band gap energy value, in other words the reducibility falls passing from semiconducting oxides to insulating ones. The previous observation is thus in agreement with the dramatic band gap narrowing observed moving from bare zirconia to ZT10 and ZT15 materials. A further consideration can be made concerning the formation of reduced titanium centers. In a computational study of the tetragonal  $\text{TiO}_2\text{-ZrO}_2$  system, Gallino et al<sup>40</sup> have shown that Ti dopants in the substitutional position to Zr cause the formation of an empty Ti 3d band about 0.5 eV below the bottom of the  $\text{ZrO}_2$  conduction band. A shift of the band gap transition roughly consistent with our experimental observation was calculated. The formation of  $\text{Ti}^{3+}$  species in annealed Ti-doped  $\text{ZrO}_2$ , as probed also in the present work by EPR, can thus be rationalized as the result of excess electron transfer from oxygen vacancies formed by oxygen depletion, to substitutional  $\text{Ti}^{4+}$  centers whose

energy is therefore lower than that of other possible defects such as electron trapped in oxygen vacancies or reduced  $Zr^{3+}$  ions.

The mechanism is shown in the two following equations which adopt for the oxygen vacancy the well known Kröger-Vink notation:



The low energy of  $Ti^{3+}$  centers explains also the higher reducibility of the mixed solid with respect to bare or low loaded zirconia. The formation of relatively deep defect centers ( $Ti^{3+}$ ) playing the role of excess electrons stabilizers favours, in fact, the reduction process decreasing the electronic energy of the whole reduced doped solid. The same effect is observed in the case of poorly doped materials (ZT01, ZT1) or of bare  $ZrO_2$ .

Some caution has to be maintained, however, on this picture since we cannot assume that all reduced centres in the system are necessarily paramagnetic and, overall, EPR visible. For this reason a second check on the effective state of reduction of all materials has been based on the reoxidation of the reduced sample by oxygen adsorption at room temperature. In such mild conditions (the spectra obtained are shown in figure 7A) electron transfer, at least partially, occurs from the solid to the adsorbed molecule with the main formation of superoxide radical ions ( $O_2^-$ ). Samples ZT01 and ZT1 behave like the bare oxide. A weak signal of adsorbed superoxide having rhombic symmetry ( $g_{zz}=2.035-2.032$ ,  $g_{yy}=2.010$  and  $g_{xx}=2.003$ ) is formed in these three cases. It is well known that the  $g_{zz}$  value of an ionic superoxide is sensitive to the nature and environment of the adsorbing cation<sup>41</sup>. In particular the z component of the g tensor is :

$$g_{zz} = g_e + 2\lambda / \Delta \quad (3)$$

the z direction being along the internuclear axis.  $\Delta$  is the separation between the two  $\pi$  antibonding orbitals of the adsorbed molecule and  $\lambda$  is the spin orbit coupling constant of oxygen, generally assumed to be  $135 \text{ cm}^{-1}$ . The magnitude of the  $g_{zz}$  component can be used as a probe of the oxide surface since it gives a measure of the cation charge at the adsorption site<sup>41, 42</sup>. Where only one charge state of the cation is expected the various  $g_{zz}$  values correspond to adsorption sites where the effective crystal field is changed either as a result of different crystal planes and/or different local coordination.

In the cases of the low Ti loading samples there is no doubt that the main adsorbing centres are surface  $Zr^{4+}$  sites<sup>19, 36-39, 41, 43-45</sup>. Remarkably, the more intense  $g_{zz}$  component shifts at lower values (from  $g = 2.035$  to  $g = 2.032$ , Fig. 7B) moving from Z to ZT1 indicating a tiny modification of the

coordinative environment of surface zirconium ions acting as adsorption sites which parallels the compositional change. ZT10 and ZT15 samples show a different signal after oxygen adsorption. The superoxide signal is more intense than in the two previous cases and part of the reduced  $Ti^{3+}$  centres are not consumed by oxygen adsorption. This result confirms what was already hypothesized in this Section, i.e. that the reducibility of the materials is proportional to the Ti content. Looking to the  $g_{zz}$  spectral region in these two cases (Fig.5, d and e), another important feature has to be emphasized. ZT10 and ZT15 have  $g_{zz}$  components which are clearly different from those measured for the low loading materials, the main components being at  $g=2.022$  and  $g=2.027$ . Both signals have to be assigned to a superoxide anion adsorbed onto a  $Ti^{4+}$  ion<sup>41, 42, 46</sup>, a tetravalent ion like  $Zr^{4+}$  but with a smaller size than the previous one and, hence, a higher charge/volume ratio and a lower  $g_{zz}$  (Equation 3). These results indicate that, at higher Ti loading,  $Ti^{4+}$  ions become the preferential adsorption sites at the surface. This is due not only to the more favourable charge/volume ratio with respect to  $Zr^{4+}$  (implying higher adsorption energy) but also to the higher  $Ti^{4+}/Zr^{4+}$  ratio, with respect to the nominal one, occurring at the surface as indicated by comparison of XPS and ICP results (*vide supra*).

Fig. 7

#### 4. Conclusions

$ZrO_2$ - $TiO_2$  mixed systems were prepared using a sol-gel synthesis that leads to the formation of solid solutions of the two oxides (ZTn materials) at least till a molar fraction of 15%  $TiO_2$  in  $ZrO_2$ . After preparation the solids were calcined at high temperature in order to obtain thermodynamically stable phases. The thermal process aims at the formation of a pure monoclinic phase for zirconia. While in the low loaded systems (0-1%) the monoclinic phase is dominant, the presence of higher Ti concentration favors the stabilization of a tetragonal  $ZrO_2$  phase. The solid solutions with higher Ti loading are not uniform in composition as a gradient of Ti concentration (which decreases from surface towards the bulk) is revealed comparing XPS results and chemical analysis. The ZT systems have remarkable optical properties as a remarkable red shift of the valence band to conduction band transition is observed which is proportional to the Ti content.

Oxygen depletion by annealing at high temperature occurs in all solids and is proportional to the Ti content. Therefore the higher the Ti fraction the higher the reducibility of the system. Reduction of the solids leads to the formation of  $Ti^{3+}$  centers which are distributed between the surface and the bulk of the solids. These results are in agreement with the picture proposed by

theoretical modeling which describe titanium states quite deep into the zirconia band gap. Reoxidation starts with the one electron reduction of dioxygen to superoxide. This radical anion is preferentially adsorbed on  $\text{Ti}^{4+}$  centers in the samples with high titanium loading confirming the presence of a Ti rich surface in these particular materials whose EPR signal is the same observed on thermally annealed  $\text{TiO}_2$  (anatase).

In this paper, on the one hand, we have characterized systems which are finding increasing applications in catalysis and photocatalysis. On the other hand the investigated systems, have also revealed as excellent model systems to investigate the role of impurities in modifying the band structure of a solid.

### ***Acknowledgments***

The work has been supported by the Italian MIUR through the FIRB Project RBAP115AYN “Oxides at the nanoscale: multifunctionality and applications” and by Compagnia di san Paolo through the project ORTO11RRT5 “Advances in nanostructured materials and interfaces for key technologies.”

The Raman measures have been obtained with the equipment acquired by the Interdepartmental Center “G. Scansetti” for Studies on Asbestos and Other Toxic Particulates with a grant from Compagnia di San Paolo, Torino, Italy.

## References

1. T. Yamaguchi, *Catalysis Today* **1994**, 20, (2), 199-218.
2. R. H. French; S. J. Glass; F. S. Ohuchi; Y. N. Xu; W. Y. Ching, *Physical Review B* **1994**, 49, (8), 5133-5141.
3. Q. Y. Xu; M. A. Anderson, *Journal of the American Ceramic Society* **1993**, 76, (8), 2093-2097.
4. H. Zou; Y. S. Lin, *Applied Catalysis A* **2004**, 265, (1), 35-42.
5. K. Kubo; S. Hosokawa; S. Furukawa; S. Iwamoto; M. Inoue, *Journal of Materials Science* **2008**, 43, (7), 2198-2205.
6. M. E. Manriquez; T. Lopez; R. Gomez; J. Navarrete, *Journal of Molecular Catalysis A: Chemical* **2004**, 220, (2), 229-237.
7. R. C. Chang; I. Wang, *Journal of Catalysis* **1987**, 107, (1), 195-200.
8. J. Fung; I. Wang, *Journal of Catalysis* **1991**, 130, (2), 577-587.
9. A. Arata; (sbagliato); S. Akugatawa; K. Tanabe, *Bulletin of the Chemical Society of Japan* **1976**, 49, 390.
10. K. Tanabe; T. Yamaguchi, *Catalysis Today* **1994**, 20, (2), 185-198.
11. S. Kataoka; D. T. Tompkins; W. A. Zeltner; M. A. Anderson, *Journal of Photochemistry and Photobiology A* **2002**, 148, (1-3), 323-330.
12. S. W. Liu; C. F. Song; M. K. Lu; S. F. Wang; D. L. Sun; Y. X. Qi; D. Xu; D. R. Yuan, *Catalysis Communications* **2003**, 4, (7), 343-346.
13. J. A. Navio; G. Colon; J. M. Herrmann, *Journal of Photochemistry and Photobiology A* **1997**, 108, (2-3), 179-185.
14. M. D. Hernandez-Alonso; I. Tejedor-Tejedor; J. M. Coronado; M. A. Anderson; J. Soria, *Catalysis Today* **2009**, 143, (3-4), 364-373.
15. M. D. Hernandez-Alonso; J. M. Coronado; B. Bachiller-Baeza; M. Fernandez-Garcia; J. Soria, *Chemistry of Materials* **2007**, 19, (17), 4283-4291.
16. W. Zhou; K. Liu; H. Fu; K. Pan; L. Zhang; L. Wang; C.-C. Sun, *Nanotechnology* **2008**, 19, (3).
17. K. V. R. Chary; G. V. Sagar; D. Naresh; K. K. Seela; B. Sridhar, *Journal of Physical Chemistry B* **2005**, 109, (19), 9437-9444.
18. Y. Cong; B. Li; B. Lei; W. Li, *Journal of Luminescence* **2007**, 126, (2), 822-826.
19. S. Livraghi; F. Olivero; M. C. Paganini; E. Giamello, *Journal of Physical Chemistry C* **2010**, 114, (43), 18553-18558.
20. V. C. Pandolfelli; J. A. Rodrigues; R. Stevens, *Journal of Materials Science* **1991**, 26, (19), 5327-5334.
21. M. E. Zorn; D. T. Tompkins; W. A. Zeltner; M. A. Anderson, *Applied Catalysis B* **1999**, 23, (1), 1-8.
22. M. Daturi; A. Cremona; F. Milella; G. Busca; E. Vogna, *Journal of the European Ceramic Society* **1998**, 18, (8), 1079-1087.
23. Y. H. Zhang; G. X. Xiong; N. Yao; W. S. Yang; X. Z. Fu, *Catalysis Today* **2001**, 68, (1-3), 89-95.
24. H. M. Ondik; H. F. McMurdie, in: *Phase diagrams for zirconium and zirconia systems*, H. M. Ondik; H. F. McMurdie, (Eds.) American Ceramic Society: Westerville (Ohio), 1998; pp 136-140.
25. M. Chiesa; E. Giamello; M. Che, *Chemical Reviews* **2010**, 110, (3), 1320-1347.
26. M. Chiesa; M. C. Paganini; E. Giamello; D. M. Murphy; C. Di Valentin; G. Pacchioni, *Accounts of Chemical Research* **2006**, 39, (11), 861-867.
27. L. Lutterotti; M. Bortolotti; G. Ischia; I. Lonardelli; H. R. Wenk, *Zeitschrift Fur Kristallographie* **2007**, 125-130.
28. L. Lutterotti, *Nuclear Instruments and Methods in Physical Research Section B* **2010**, 268, (3-4), 334-340.
29. D. Gazzoli; G. Mattei; M. Valigi, *Journal of Raman Spectroscopy* **2007**, 38, (7), 824-831.
30. G. Duan; X. Yang; A. Lu; G. Huang; L. Lu; X. Wang, *Materials Characterization* **2007**, 58, (1), 78-81.
31. M. J. Li; Z. H. Feng; G. Xiong; P. L. Ying; Q. Xin; C. Li, *Journal of Physical Chemistry B* **2001**, 105, (34), 8107-8111.
32. H. C. Choi; Y. M. Jung; S. B. Kim, *Vibrational Spectroscopy* **2005**, 37, (1), 33-38.
33. V. Swamy; B. C. Muddle; Q. Dai, *Applied Physics Letters* **2006**, 89, (16).
34. G. Martra; E. Gianotti; S. Coluccia, in: *Metal Oxide Catalysis*, D. D. Jackson; J. S. J. Hargreaves, (Eds.) Wiley-VCH: Weinheim, 2009; pp 51-94.

35. M. Occhiuzzi; D. Cordischi; R. Dragone, *Journal of Physical Chemistry B* **2002**, 106, (48), 12464-12469.
36. A. M. Volodin, *Catalysis Today* **2000**, 58, (2-3), 103-114.
37. A. F. Bedilo; M. A. Plotnikov; N. V. Mezentseva; A. M. Volodin; G. M. Zhidomirov; I. M. Rybkin; K. J. Klabunde, *Physical Chemistry Chemical Physics* **2005**, 7, (16), 3059-3069.
38. M. I. Ivanovskaya; E. V. Frolova, *Russian Journal of General Chemistry* **2007**, 77, (4), 524-531.
39. Q. Zhao; X. P. Wang; T. X. Cai, *Applied Surface Science* **2004**, 225, (1-4), 7-13.
40. F. Gallino; C. Di Valentin; G. Pacchioni, *Physical Chemistry Chemical Physics* **2011**, 13, (39), 17667-17675.
41. M. Che; A. J. Tench, *Advances in Catalysis* **1983**, 32, 1-148.
42. M. Anpo; M. Che; B. Fubini; E. Garrone; E. Giamello; M. C. Paganini, *Topics in Catalysis* **1999**, 8, (3-4), 189-198.
43. E. V. Frolova; M. I. Ivanovskaya, *Materials Science and Engineering C* **2006**, 26, (5-7), 1106-1110.
44. A. V. Emeline; A. V. Panasuk; N. Sheremetyeva; N. Serpone, *Journal of Physical Chemistry B* **2005**, 109, (7), 2785-2792.
45. F. Fresno; M. D. Hernandez-Alonso; D. Tudela; J. M. Coronado; J. Soria, *Applied Catalysis B* **2008**, 84, (3-4), 598-606.
46. S. Livraghi; M. C. Paganini; E. Giamello; A. Selloni; C. Di Valentin; G. Pacchioni, *Journal of the American Chemical Society* **2006**, 128, (49), 15666-15671.